Cyclopentadienyl, Indenyl, and Fluorenyl Anions: Gas-Phase and Solvation Energy Contributions to Electron Detachment Energies

Bettina Römer, Gordon A. Janaway, and John I. Brauman*

Contribution from the Department of Chemistry, Stanford University, Stanford, California 94305-5080

Received June 10, 1996[⊗]

Abstract: We have measured the gas-phase electron affinities of indenyl and fluorenyl radicals to be 42.7 ± 0.3 and 43.1 ± 0.3 kcal/mol, respectively, by electron photodetachment spectroscopy, using an ion cyclotron resonance spectrometer to generate, trap, and detect ions. From the electron affinities and literature values for the gas-phase acidities, we derive the bond dissociation energies: indene, 81.1 ± 2.4 kcal/mol and fluorene, 81.3 ± 2.4 kcal/mol. We describe a general approach for comparing gas and solution-phase ionic properties.

Introduction

Solvation plays an important role in the chemistry of ions.[1] Gas- and solution-phase data have been measured for many ions,[2,3] and while solvation effects have been studied extensively,[4] a quantitative explanation of observed trends is often difficult to rationalize. The absolute reactivity of ions in solution differs significantly from that of gas-phase ions, and the relative reactivity may differ as well. One of the best known examples of this phenomenon is the reversal in the acidities of simple aliphatic alcohols between gas and solution phase.[5] Comparisons of gas- and solution-phase properties, such as acidities or ionization potentials, often reveal linear correlations with varying, even negative, slopes.[6,7] Developing a model for the interconnectivity between gas- and solution-phase properties will aid in understanding these observations.

We chose to examine the anions of cyclopentadiene, indene, and fluorene. These compounds constitute a homologous series of non-alternant aromatic hydrocarbons with similar electronic structure but varying size. We have measured the electron affinities of the indenyl and fluorenyl radicals and, using known gas-phase acidities,[8−10] derived corresponding bond dissociation energies. These bond dissociation energies agree well with those determined previously from gas-phase and solution-phase measurements.

A plot of the electron affinities of cyclopentadiene, indene, and fluorene against their solution-phase counterparts reveals a correlation with negative slope. In contrast, linear positive slopes have been observed previously in many other systems, including ionization potentials of aromatic hydrocarbons and acidities of substituted benzoic acids. In order to explain these observations, we develop a model relating gas-phase properties and solvation effects.

Experimental Section

Ion Cyclotron Resonance Spectrometer. Experiments were performed with an ion cyclotron resonance (ICR) spectrometer, in which ions were continuously generated and detected.[11] The continuous mode detection provided a large signal-to-noise ratio which allowed detection of small changes (less than 1%) in the ion population. A home-built capacitance bridge detector[12] allowed detection at a single frequency. A frequency lock[12] was employed to compensate for light-induced frequency shifts, ensuring that the signal was always measured at its maximum.

Light Sources. A 1000-W Xe arc lamp (Canrad-Hanovia) with a 0.25-m grating monochromator (Kratos Analytical) was used as a light source for the low-resolution photodetachment spectra. The monochromator was calibrated using a wavelength reversion spectroscope (Beck) and the output of the calibrated laser system (see below), resulting in a band width of about 20 nm. A power spectrum was measured by directing the beam into a thermopile (Eppley Laboratory, Inc.) either immediately before or after data collection. The output of the thermopile was amplified, then digitized and recorded using a 12-bit A/D converter on an IBM Data Acquisition and Control Adapter Board, mounted in an IBM XT.

High-resolution spectra were obtained using a tunable dye laser (Coherent 590) pumped by an Ar-ion laser (Innova 200/15). Wavelengths were selected using a three-plate birefringent filter (band width ±1 cm^{-1}). The laser dyes DCM and Rhodamine 6G (Exciton) were used, and the output of the dye laser was calibrated with a Ca/Ne optogalvanic lamp (Perkin Elmer). The current of the lamp changes when the wavelength of the laser matches an electronic transition of the atoms in the lamp, and the laser was calibrated by comparing these measured transitions to known values.[13] To allow power measurement during data collection, about 3% of the laser light was split off and directed into the thermopile.

[⊗] Abstract published in *Advance ACS Abstracts,* February 1, 1997.

(1) March, J. *Advanced Organic Chemistry*, 4th ed.; John Wiley & Sons: New York, 1992; pp 269−272.
(2) Bartmess, J. E. NIST Negative Ion Energetics Database, Version 3.0; Standard Reference Database 19B, National Institute of Standard Technology, 1993.
(3) Bordwell, F. G. *Acc. Chem. Res.* **1988**, *21*, 456−463.
(4) Dyumaev, K. M.; Korolev, B. A. *Russ. Chem. Rev.* **1980**, *49*, 1021−1032.
(5) Brauman, J. I.; Blair, L. K. *J. Am. Chem. Soc.* **1970**, *92*, 5986−5992.
(6) McMahon, T. B.; Kebarle, P. *J. Am. Chem. Soc.* **1977**, *99*, 2222−2230.
(7) Streitwieser, A., Jr. *Progress in Physical Organic Chemistry*; Cohen, S. G., Streitwieser, A., Jr., Taft, R. W., Eds.; Interscience Publishers: New York, 1963; Vol. 1, pp 1−30.
(8) McMillen, D. F.; Golden, D. M. *Annu. Rev. Phys. Chem.* **1982**, 33.
(9) Bartmess, J. E.; Scott, J. A.; McIver, R. T., Jr *J. Am. Chem. Soc.* **1979**, *101*, 6047−6056.
(10) Taft, R. W.; Bordwell, F. G. *Acc. Chem. Res.* **1988**, *21*, 463−469.
(11) Lehman, T. A.; Bursey, M. M. *Ion Cyclotron Resonance Spectrometry*; Wiley-Interscience: New York, 1976.
(12) Marks, J.; Drzaic, P. S.; Foster, R. F.; Wetzel, D. M.; Brauman, J. I.; Uppal, J. S.; Staley, R. H. *Rev. Sci. Instrum.* **1987**, *58*, 1460−4163.
(13) *M.I.T. Wavelength Tables—Wavelengths by Element*; M.I.T. Press: Cambridge, 1982; Vol. 2.
(14) Zimmerman, A. H. Ph.D. Thesis, Stanford University, 1977.

S0002-7863(96)01947-6 CCC: $14.00

Data Acquisition and Analysis. Photodetachment spectra were obtained by monitoring decreases in ion signal as a function of the wavelength of incident light, digitized, and recorded by the IBM XT described above. The neutral pressure during each of these experiments was maintained at about 10^{-7} Torr, with ions continuously being generated and detected. Before and after each experiment, a baseline reading of the ion signal without incident light was recorded. When light was allowed to enter the cell, a 4-s delay before data collection at each new wavelength allowed for the re-establishment of an equilibrium ion population. The ion signal was then monitored for 2 s (15 000 readings), and the average value recorded before the wavelength of the incident light was incremented. Low-resolution data were collected at intervals of 10 nm, while high-resolution data were recorded in 1-nm steps. Spectra were collected over a period of at most 10 min to control drift in the baseline signal.

Fractional decreases were calculated from the ion signal intensity with and without light:

$$F(\lambda) = \frac{I_{\text{light off}} - I_{\text{light on}}}{I_{\text{light off}}} \quad (1)$$

Normalized cross sections were calculated from the wavelength (λ) and intensity (I) of incident light and the fractional ion decrease using the steady-state model:[14]

$$\sigma(\lambda) \propto \frac{F(\lambda)}{I\lambda[1 - F(\lambda)]} \quad (2)$$

A minimum of three scans were averaged for every wavelength region. These regions were chosen to overlap with one another so that they could be spliced together to produce the photodetachment spectra reported here.

Materials. Indene and fluorene were purchased from Aldrich; nitrogen trifluoride was purchased from Ozark-Mahoning. All compounds were degassed by several freeze−pump−thaw cycles before they were introduced into the high-vacuum chamber.

Ion Generation. Fluoride ion was generated by impact of low-energy (less than 1 eV) electrons on nitrogen trifluoride:

$$NF_3 + e^- \rightarrow F^- + NF_2 \quad (3)$$

Fluoride ion then abstracted the acidic proton of indene to form indenyl anion.

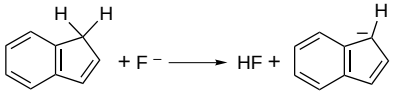

(4)

Fluorenyl anion was formed similarly via proton abstraction from fluorene by F^-.

Results

Onset. Indenyl and fluorenyl photodetachment thresholds were determined by linear extrapolation to zero cross section. The low-resolution spectrum of indenyl anion (Figure 1) displays a photodetachment threshold at 675 nm. Correcting for the band width of the monochromator, we estimate the low-resolution onset to be 655 ± 20 nm. The high-resolution spectrum (Figure 2) displays a threshold at 669 nm. By identifying the maximum and minimum possible values for the onset by linear extrapolation of selected points, the error limits were estimated to be ±5 nm.

The low-resolution spectrum of fluorenyl anion (Figure 3) displays an apparent photodetachment onset at 665 nm, yielding an estimate for the threshold of 645 ± 20 nm. The photodetachment threshold appears at 665 nm in the high-resolution spectrum (Figure 4), with error limits estimated to be ±5 nm. We attribute the small amount of photodetachment observed at wavelengths above 665 nm to the presence of a hot band, representing photodetachment from vibrationally excited fluorenyl anions at an energy 0.4 kcal/mol (0.02 eV) above the ground state.

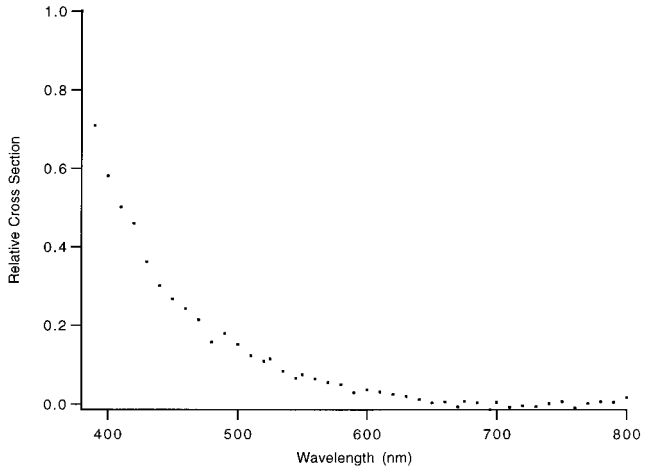

Figure 1. Low-resolution photodetachment spectrum of indenyl anion (spectral band width of 20 nm).

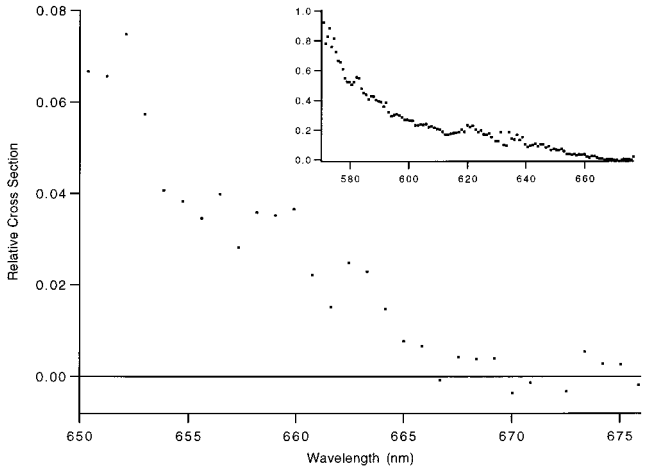

Figure 2. High-resolution photodetachment spectrum of indenyl anion with the entire threshold region shown in the inset.

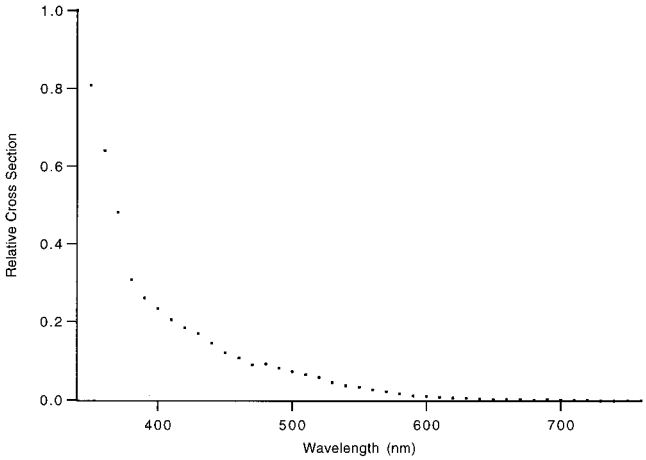

Figure 3. Low-resolution photodetachment spectrum of fluorenyl anion (spectral band width of 20 nm).

The calculated geometries[15] of each anion and its corresponding radical are similar, implying that the Franck−Condon

(15) AM1 and 6-31G* calculations were performed using the Spartan Molecular Modelling Package. The Restricted Hartree−Fock (RHF) model was used to calculate anion geometries, and the Unrestricted Hartree−Fock (UHF) model was used for radical geometries.

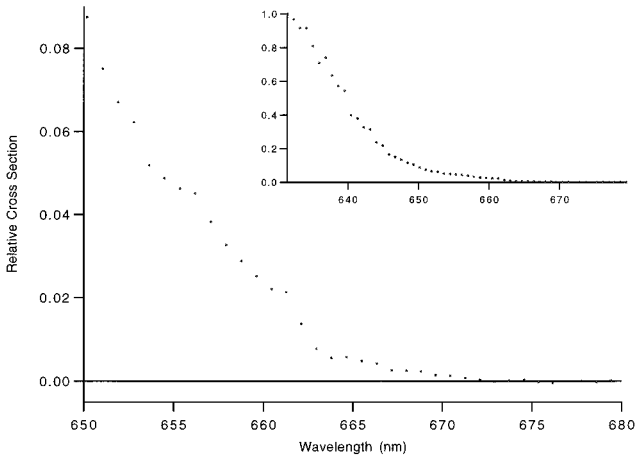

Figure 4. High-resolution photodetachment spectrum of fluorenyl anion with the entire threshold region shown in the inset.

Table 1. Electron Affinities, Acidities, and Bond Dissociation Energies[a]

R	EA(A•)	ΔH_{acid}(AH)	BDE(AH)
cyclopentadiene	41.2 ± 0.44[b]	353.9 ± 2.2[c]	81.5 ± 2.7
indene	42.7 ± 0.3	352.0 ± 2.1[d]	81.1 ± 2.4
fluorene	43.0 ± 0.3	351.8 ± 2.1[d]	81.2 ± 2.4

[a] All values in kcal/mol. [b] Reference 16. [c] Reference 9. [d] Reference 10.

overlap is large. Thus the detachment energy observed should correspond to the adiabatic electron affinity of the radical. Therefore, we assign the electron affinity of indenyl radical as 1.853 ± 0.014 eV (42.7 ± 0.3 kcal/mol) and the electron affinity of fluorenyl radical as 1.864 ± 0.014 eV (43.0 ± 0.3 kcal/mol).

High-Energy Region. The low-resolution photodetachment spectrum of indenyl anion displays a steadily increasing cross section. The spectrum of fluorenyl anion shows a weak, but reproducible, resonance between 480 and 500 nm.

Discussion

Electron Affinities. The electron affinities of indenyl and fluorenyl radical are listed in Table 1, and the electron affinity for cyclopentadienyl radical[16] is included for comparison. The electron affinities of each are similar, although they increase slightly with increasing size.

Bond Dissociation Energies. The homolytic bond dissociation energy (BDE) of a neutral hydrocarbon can be expressed as a function of its gas-phase acidity (ΔH_{acid}) and electron affinity (EA):

$$\mathrm{BDE(AH)} = \mathrm{EA(A^\bullet)} + \Delta H_{acid}\mathrm{(AH)} - \mathrm{IP(H^\bullet)} \qquad (5)$$

The ionization potential of hydrogen[17] and the gas-phase acidities[2] of cyclopentadiene, indene, and fluorene are known. The resulting bond dissociation energies are listed in Table 1.

The bond dissociation energies we report agree well with values found in the literature. Benson has measured the C−H bond dissociation energy for cyclopentadiene to be 81.2 ± 1.2 kcal/mol,[18] and Rüchardt has reported a value of 81.9 kcal/mol for the bond dissociation energy of fluorene.[19] DeFrees has reported a value of 82.9 ± 2.2 kcal/mol, obtained by bracketing the gas-phase proton affinity of cyclopentadienyl radical, and then combining this value with the previously measured ionization potential.[20] The only gas-phase measurement of the bond dissociation energy of indene, measured by Stein, is 84 ± 3 kcal/mol.[21]

Table 2. Gas-Phase and Solution Electron Detachment Energies[a]

R	gas-phase EA(A•)	solution $\Delta E_{ox}(A^-)$[b]
cyclopentadiene	1.786[c]	0.028
indene	1.853	−0.202
fluorene	1.864	−0.319

[a] All values in eV. [b] Measured in DMSO, ref 21. [c] Reference 17.

Using a thermochemical relationship analogous to eq 5, Bordwell determined bond dissociation energies for these compounds using solution-phase measurements of their redox potentials and pK_{HA} values.[22] Arnett has confirmed these values.[23] Estimating that the solvation energy of the neutral molecule is equal to that of the radical, and correcting for the solvation energy of the hydrogen atom, Bordwell derived "gas-phase" bond dissociation energies. His values are 81.2 ± 3, 78.8 ± 3, and 79.5 ± 3 kcal/mol for cyclopentadiene, indene, and fluorene, respectively, which are equal within experimental error and agree with our values within experimental error.

Gas-Phase Versus Solution-Phase Values. The process of gas-phase electron detachment can be compared to solution-phase electrochemical oxidation; in both cases, a closed-shell anion is converted to a radical upon loss of an electron. The thermodynamics of this simple process depend greatly on the structural and dielectric environments in which it occurs, and in general, the relationship between electron affinity and oxidation potential can be difficult to predict. However, linear correlations have been observed among homologous sets of compounds,[10,24] and in order to explain these trends it is necessary to identify factors which contribute to the thermodynamics of each process.

The electron affinities of cyclopentadienyl, indenyl, and fluorenyl radicals are shown in Table 2, as are the oxidation potentials of the corresponding anions in DMSO.[22] The electron affinities increase slightly in the order cyclopentadiene, indene, fluorene, whereas the solution-phase trend is reversed. These values are plotted in Figure 5. The correlation has a slope of about −0.2.

For comparison, consider alternant aromatic hydrocarbons, where the energy associated with removal of an electron corresponds to the ionization potential in the gas phase and the oxidation potential in solution. The gas-phase ionization potentials[25] and solution oxidation potentials[26] of the following representative compounds are plotted in Figure 6: benzene, naphthalene, anthracene, tetracene, phenanthrene, pyrene, and 1,2-benzopyrene. The least-squares fit to these data has a slope of +1.6.

(16) Engelking, P. C.; Lineberger, W. C. *J. Chem. Phys.* **1977**, *67*, 1412−1417.
(17) Chase, M. W., Jr.; Davies, C. A.; Downey, J. R., Jr.; Frurip, D. J.; McDonald, R. A.; Syverud, A. N. *J. Phys. Chem. Ref. Data* **1985**, *14*, *Suppl. 1*, 1211.
(18) Furuyama, S.; Golden, D. M.; Benson, S. W. *Int. J. Chem. Kinet.* **1971**, *3*, 237−248.
(19) Rakus, K.; Verevkin, S. P.; Schätzer, J.; Beckhaus, H.; Rüchardt, C. *Chem. Ber.* **1994**, *127*, 1095.
(20) DeFrees, D. J.; McIver, R. T., Jr.; Hehre, W. J. *J. Am. Chem. Soc.* **1980**, *102*, 3334−3338.
(21) Stein, S. E. *New Approaches in Coal Chemistry*; Blaustein, B. D., Bockrath, B. C., Friedman, S., Eds.; American Chemical Society: Washington, DC, 1981; Vol. 169, p 97.
(22) Bordwell, F. G.; Cheng, J.-P.; Harrelson, J. A., Jr. *J. Am. Chem. Soc.* **1988**, *110*, 1229−1231.
(23) Arnett, E. M.; Moriarity, T. C.; Small, L. E.; Rudolph, J. P.; Quirk, R. P. *J. Am. Chem. Soc.* **1973**, *95*, 1492−1495.
(24) Arnett, E. M.; Venkatasubramaniam, K. G. *J. Org. Chem.* **1983**, *48*, 1569−1578.
(25) Lias, S. G.; Bartmess, J. E.; Liebman, J. F.; Holmes, J. L.; Levin, R. D.; Mallard, W. G. *J. Phys. Chem. Ref. Data* **1988**, *17*, *Suppl. No. 1*.
(26) Streitwieser, A., Jr. *Molecular Orbital Theory for Organic Chemists*; John Wiley & Sons, Inc.: New York, 1961.

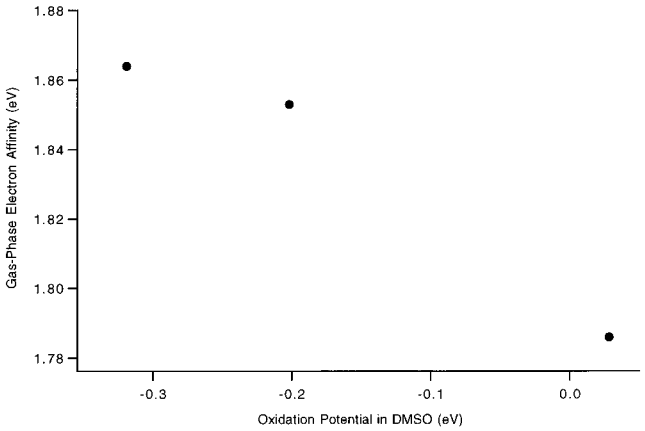

Figure 5. Gas-phase electron affinities and solution oxidation potentials of cyclopentadienyl, indenyl, and fluorenyl radicals.

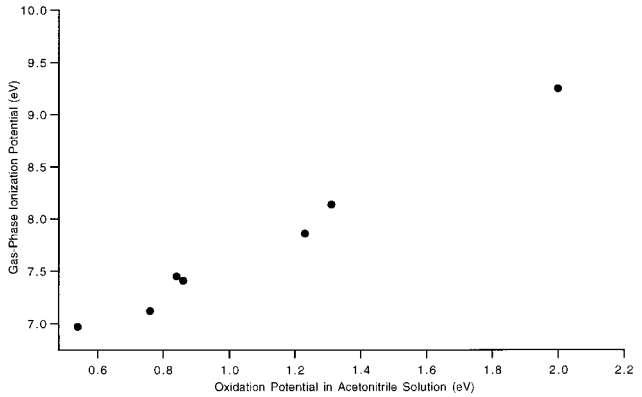

Figure 6. Gas-phase ionization potential vs solution oxidation potential for several alternant aromatic hydrocarbons (see text).

Equation 6 relates the energy associated with electron loss in the gas phase to the energy for the same process in solution.[26,27]

$$\Delta E_{\text{solution}} = \Delta E_{\text{gas}} + \Delta\Delta E_{\text{solvation}} \tag{6}$$

where $\Delta\Delta E_{\text{solvation}}$ is the difference between the solvation energies of the ion and neutral. As Streitwieser has noted,[26] a linear correlation between gas-phase and solution-phase properties implies that $\Delta\Delta E_{\text{solvation}}$ is proportional to ΔE_{gas}:

$$\Delta E_{\text{solution}} = k\Delta E_{\text{gas}} \tag{7}$$

implies

$$\Delta\Delta E_{\text{solvation}} = (k-1)\Delta E_{\text{gas}} \tag{8}$$

Extending Streitwieser's analysis, proportionality between gas-phase energy and solvation energy (Equation 8) within a homologous series suggests that both quantities are tracking the same physical parameter. For both series of aromatic hydrocarbons, the appropriate physical property seems to be size—expressible, for example, as an average ionic radius.

Parametric dependence of solvation energy on ionic size can be modeled to first-order using Born charging, in which the solvation energy ($\Delta G^\circ_{\text{solv}}$) of a charged sphere embedded in a dielectric (dielectric constant D) is inversely proportional to the radius (r_o) of the sphere.

$$\Delta G^\circ_{\text{solv}} = \frac{Ne^2}{8\pi\epsilon_o r_o}\left(1 - \frac{1}{D}\right) \tag{9}$$

where N is Avogadro's number, e the electronic charge, and ϵ_o the permittivity of free space. Although more sophisticated solvent models could be applied in this analysis, the Born model is sufficient for discussing general trends in size dependence.

We find that the ionization potentials (ΔE_{gas} values) of alternant aromatic hydrocarbons depend inversely on ionic radius, as shown in Figure 7.[7,25,26,28] This approximately linear trend is easily understood. The ionization potential is a function of the energy of the highest occupied molecular orbital, the HOMO.[7,25,26] In general, the bonding and antibonding molecular orbital energies are symmetrically disposed in alternant aromatic hydrocarbons. As the molecule increases in size the HOMO energy increases (i.e., the binding energy decreases), and thus the ionization potential decreases, yielding the slope observed in Figure 7.

Rewriting Equation 6 for the example of the alternant aromatic hydrocarbons,

$$\epsilon_{\text{ox}} = \text{IP} + \Delta G^\circ_{\text{solv}} \tag{10}$$

where ϵ_{ox} is the half-wave oxidation potential, IP is the ionization potential, and $\Delta G^\circ_{\text{solv}}$ is the ion solvation energy.[29] Ionization potential is inversely dependent on size, Figure 7, so that

$$\text{IP} = k_1/r \tag{11}$$

$\Delta G^\circ_{\text{solv}}$ is inversely dependent on the radius, eq 9, so that

$$\Delta G^\circ_{\text{solv}} = \frac{-k_2}{r} = -\left(\frac{k_2}{k_1}\right)\text{IP} \tag{12}$$

where k_1 and k_2 are defined as positive quantities. The half-wave oxidation potential can then be related to the ionization potential:

$$\text{IP} = \left(\frac{k_1}{k_1 - k_2}\right)\epsilon_{\text{ox}} \tag{13}$$

The slope of +1.56 (Figure 6) indicates that the IP sensitivity to size, k_1, is about three times larger than the $\Delta G^\circ_{\text{solv}}$ sensitivity to size, k_2.

Relationships similar to eq 13 can be derived for other measures of energy differences, and for different sets of homologous compounds. For example, a linear correlation between gas-phase and solution-phase acidities of substituted benzoic acids is observed; both acidities depend in part on the same variable, the Hammett parameter σ.[6,30] A benzoic acid with a strongly electron-withdrawing substituent will deprotonate more readily in the gas phase than will a benzoic acid with a less strongly electron-withdrawing substituent.[7] The substituent causes the charge to be more dispersed, and in solution a more dispersed charge will be less solvated than a more concentrated charge. A plot of gas-phase against solution-phase acidities yields a linear slope of about 10 for benzoic acids,[6] indicating

(27) We have omitted a third ΔE term from the expression on the right of this equation, representing the solvation energy of a free electron. This term is a constant which does not affect the energy trends discussed here.

(28) We plot here a series of alternant aromatic hydrocarbons increasing in molecular size: benzene, naphthalene, anthracene, tetracene, pentacene.

(29) The $\Delta\Delta E$ term of eq 6 represents the differential solvation energy of the ion and neutral. The solvation energies of the neutrals discussed here are expected to be small compared to those of the ions, and are not expected to change dramatically within a homologous set of compounds. We have therefore chosen to examine the parameter which dominates this term, the free energy of solvation of the ion.

(30) Taft, R. W., Jr. *J. Phys. Chem.* **1960**, *64*, 1805−1815.

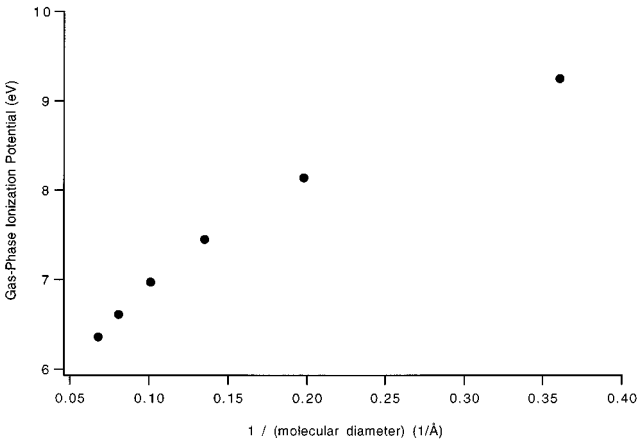

Figure 7. Gas-phase ionization potential as a function of molecular size for several alternant aromatic hydrocarbons (see text).

that k_2 is about 0.9 k_1. Similar behavior is observed in the acidities of substituted phenols, yielding a slope of about 7.

If solvation energy differences are larger than those of gas-phase energy differences, k_2 is larger than k_1 and eq 13 predicts a negative slope. This is observed, for example, when comparing gas-phase and solution-phase acidities of small aliphatic alcohols.[5] Gas-phase acidity increases in the order of methanol, ethanol, propanol, *tert*-butyl alcohol; in solution, however, the order is reversed. Thus, even though *tert*-butyl alcohol is the most acidic in the gas phase, its anion is solvated significantly less than methoxide, which results in a decreased acidity in solution. Sufficient variation in solvation energy can thus not only attenuate energy differences in acidities but even cause a reversal in the gas-phase order.[31]

Returning to the series cyclopentadiene, indene, and fluorene, the slope of about −0.23 (Figure 5) indicates that the magnitude of k_2 is several times that of k_1. That k_1 is small can be seen in Table 2, where ionic size has little effect on the gas-phase electron affinities of these molecules. This weak dependence can be rationalized by noting that in contrast to alternant systems, non-alternant systems do not necessarily have symmetrically-spaced molecular orbital energy levels. Hence an increase in size and the accompanying increase in the number of molecular orbitals do not necessarily correlate with electron affinity. However, the sensitivity to size of the solvation energy, k_2, remains large, implying that solvation energy is the dominant term contributing to the relative oxidation potentials ($\Delta\Delta E_{solution}$) of cyclopentadiene, indene, and fluorene.

Instead of comparing gas and solution energies, one could examine trends in the thermodynamic properties of ions in different solvent environments. Arnett, for example, has observed many such correlations.[24] In the above discussion, we are seeking to provide a general framework for interpreting such results, rather than adding to this growing list of linear relationships. In other words, if indeed a correlation of anion energy is observed in two different solvents, this does not mean that the intrinsic energy of the process follows the same trend. It may be found, in fact, that k_2 is much larger than k_1, such that ΔG_{solv} in each solvent tracks the same parameter, while the gas-phase quantity is comparatively constant across the series.

Electronic States. In the photodetachment spectrum of fluorenyl anion, we observe a weak, but reproducible, resonance between 480 and 500 nm—the spectrum differs from a typical monotonic cross section curve by increasing initially and then decreasing again. Such resonances have previously been observed above the photodetachment threshold.[32−40] We believe that the structure does not arise from direct photodetachment from lower-lying molecular orbitals resulting in an electronically excited state of the neutral, because such a transition would display a steadily rising cross section curve. Instead, this resonance is attributed to transitions to an electronically excited anion state embedded in the continuum. The mixing of this discrete state with the continuum of free-electron states would enhance the probability of photon absorption over a small energy range, and the subsequent autodetachment of an electron would result in a greater decrease in ion signal.

The solution absorption spectra of several alkali salts of fluorenyl anion have been recorded.[41−44] Fluorenyl anion shows a strong absorption around 360−370 nm with a weaker band around 500 nm, indicating the presence of an excited state of the anion near the energy of the resonance observed in the photodetachment spectrum. Such absorbances in large delocalized anions typically correspond to π to π^* transitions, and molecular orbital calculations show electronic levels at similar energies.[45,46] The resonance in the photodetachment spectrum is weak, suggesting that the transition probability relative to that of direct photodetachment to the continuum is small. This conclusion is consistent with the small absorption observed for the fluorenyl anion around 500 nm in solution. The stronger solution absorption band near 360 nm was not observed in our experiments due to interference from photodetachment of fluoride (F^-) ion.

Solvent and counterion affect the exact position of solution absorption bands; for example, a more polar solvent or a smaller cation shifts the fluorenyl absorption bands to lower energies. These energy shifts are attributed to varying amounts of solvation of the cation.[43,47] When the cation is poorly solvated, ion-contact pairs exist in solution. With increasing solvation, charge separation increases and solvent-separated pairs are more common.[48] In principle, the shift between solution-phase absorption bands and gas-phase photodetachment resonances

(31) Toñón, I.; Silla, E.; Pascual-Ahuir, J.-L. *J. Am. Chem. Soc.* **1993**, *115*, 2226−2230.

(32) Richardson, J. H.; Stephenson, L. M.; Brauman, J. I. *J. Chem. Phys.* **1975**, *62*, 1580−1582.

(33) Zimmerman, A. H.; Reed, K. J.; Brauman, J. I. *J. Am. Chem. Soc.* **1977**, *99*, 7203−7209.

(34) Zimmerman, A. H.; Gygax, R.; Brauman, J. I. *J. Am. Chem. Soc.* **1978**, *100*, 5595−5597.

(35) Zimmerman, A. H.; Brauman, J. I. *J. Chem. Phys.* **1977**, *66*, 5823−5825.

(36) Jackson, R. L.; Zimmerman, A. H.; Brauman, J. I. *J. Chem. Phys.* **1979**, *71*, 2088−2094.

(37) Wetzel, D. M.; Salomon, K. E.; Brauman, J. I. *J. Am. Chem. Soc.* **1989**, *111*, 3835−3841.

(38) Drzaic, P. S.; Brauman, J. I. *J. Phys. Chem.* **1984**, *88*, 5285−5290.

(39) Gygax, R.; McPeters, H. L.; Brauman, J. I. *J. Am. Chem. Soc.* **1979**, *101*, 2567-2570.

(40) Mock, R. S.; Grimsrud, E. P. *J. Am. Chem. Soc.* **1989**, *111*, 2861−2870.

(41) Hogen-Esch, T. E.; Smid, J. *J. Am. Chem. Soc.* **1966**, *88*, 307−318.

(42) Pascault, J. P.; Golé, J. *J. Chim. Phys.* **1971**, *68*, 442.

(43) Hogen-Esch, T. E.; Plodinec, M. J. *J. Phys. Chem.* **1976**, *80*, 1090−1093.

(44) Streitwieser, A., Jr.; Brauman, J. I. *J. Am. Chem. Soc.* **1963**, *85*, 2633−2636.

(45) Häfelinger, V. G.; Streitwieser, A., Jr.; Wright, J. S. *Ber. Bunsenges. Phys. Chem.* **1969**, *73*, 456−465.

(46) Zander, M.; Fratev, F.; Olbrich, G.; Polansky, O. E. *Z. Naturforsch.* **1975**, *30A*, 1700.

(47) Vos, H. W.; MacLean, C.; Velthorst, N. H. *J. Chem. Soc., Faraday Trans. 2* **1976**, *72*, 63−75.

(48) Indenyl anion shows several weak absorption bands at wavelengths shorter than 360−370 nm, but the photodetachment spectrum is difficult to record below wavelengths of 380 nm because of photodetachment of the primary ion, F^-.

reflects the difference in electronic transition energies between solvated ion-pairs and free ions; unfortunately, the resonance observed in our spectrum is not resolved well enough to determine its exact position.

Conclusions

We have measured the electron photodetachment spectra of indenyl and fluorenyl anions, from which we have determined the electron affinities of the corresponding radicals and the bond dissociation energies of the corresponding neutrals. Comparison of gas-phase with solution-phase data reveals the magnitude of solvation effects. We develop a model to illustrate the dependence of both gas and solution properties on ionic size and extent of charge distribution.

Acknowledgment. We are grateful to the National Science Foundation for support of this research. We thank A. H. Zimmerman and C. M. Rynard for preliminary work.

JA961947X